

Distinct pressure evolution of superconductivity and charge-density-wave in kagome superconductor CsV_3Sb_5 thin flakes

Ge Ye,¹ Mengwei Xie,¹ Chufan Chen,¹ Yanan Zhang,¹ Dongting Zhang,¹ Xin Ma,¹ Xiangyu Zeng,² Fanghang Yu,³ Yi Liu,⁴ Xiaozhi Wang,⁵ Guanghan Cao,^{6,7} Xiaofeng Xu,⁴ Xianhui Chen,³ Huiqiu Yuan,^{1,7} Chao Cao,^{1,*} and Xin Lu^{1,†}

¹*Center for Correlated Matter, School of Physics, Zhejiang University, Hangzhou 310058, China*

²*Hangzhou Institute of Technology, Xidian University, Hangzhou, 311200, China*

³*CAS Key Laboratory of Strongly-coupled Quantum Matter Physics, Department of Physics, University of Science and Technology of China, Hefei, 230022, China*

⁴*Key Laboratory of Quantum Precision Measurement of Zhejiang Province, Department of Applied Physics, Zhejiang University of Technology, Hangzhou, 310014, China*

⁵*College of Information Science and Electronic Engineering, Zhejiang University, Hangzhou, 310058, China*

⁶*School of Physics, Zhejiang University, Hangzhou, 310058, China*

⁷*State Key Laboratory of Silicon and Advanced Semiconductor Materials, Zhejiang University, Hangzhou, 310058, China*

(Dated: February 12, 2024)

It is intriguing to explore the coexistence and (or) competition between charge-density-wave (CDW) and superconductivity (SC) in many correlated electron systems, such as cuprates[1–3], organic superconductors[4, 5] and dichalcogenides[6, 7]. Among them, the recently discovered \mathbb{Z}_2 topological kagome metals AV_3Sb_5 ($A=\text{K}, \text{Rb}, \text{Cs}$) serve as an ideal platform to study the intricate relation between them. Here, we report the electrical resistance measurements on CsV_3Sb_5 thin flakes (≈ 60 nm) under hydrostatic pressure up to 2.12 GPa to compare its pressure phase diagram of CDW and SC with its bulk form. Even though the CDW transition temperature (T_{CDW}) in CsV_3Sb_5 thin flakes is still monotonically suppressed under pressure and totally vanishes at $P_2=1.83$ GPa similar to the bulk, the superconducting transition temperature (T_c) shows an initial decrease and consequent increase up to its maximum ~ 8.03 K at P_2 , in sharp contrast with the M-shaped double domes in the bulk CsV_3Sb_5 . Our results suggest the important role of reduced dimensionality on the CDW state and its interplay with the SC, offering a new perspective to explore the exotic nature of CsV_3Sb_5 .

The recently discovered kagome family AV_3Sb_5 ($A=\text{K}, \text{Rb}, \text{Cs}$) with a frustrated geometry have attracted great interest due to the rich interplay between electronic correlations, topology, unconventional charge-density-wave (CDW), and superconductivity (SC) [8–11]. All members in the AV_3Sb_5 family show a superconducting state below T_c of 2.5, 0.92, and 0.93 K for $A=\text{Cs}, \text{Rb}$, and K , respectively [9–11], while the corresponding charge order emerges at T_{CDW} of 94, 102, 78 K, respectively [12–14]. Scanning tunneling microscopy (STM)[15–18], X-ray diffraction (XRD) [13] and ARPES [19–21] experiments have all revealed a 2×2 charge modulation in the V-based kagome lattice layers below T_{CDW} . Further ARPES [22], XRD [23, 24] and NMR measurements [25] have proposed a $2 \times 2 \times 2$ or $2 \times 2 \times 4$ CDW order with the stacking of star-of-David (SoD) or tri-hexagonal (TrH) distortions along the c axis, favoring a 3D nature of the CDW due to interlayer couplings. Additional breaking of time-reversal and rotational symmetry were also reported in the CDW state and an electronic origin of the CDW state has been claimed to be probably associated with the Fermi surface nesting between van Hove saddle-points at M points [26–28].

In particular, the Cs compound has the highest T_c at ambient pressure and displays a complex superconducting phase diagram compared with other members, where the bulk CsV_3Sb_5 shows a monotonic decrease of T_{CDW} till 2 GPa, and a puzzling M-shaped double-dome fea-

ture of superconductivity where the T_c peaks at $P_1^b \sim 0.7$ GPa and $P_2^b \sim 2.0$ GPa, respectively, as shown in Fig.1(b) [12, 29]. Recent NMR experiments [30] argued that a stripe-like CDW order should replace the original one at P_1^b with domain walls and be totally suppressed at P_2^b , yielding a double-dome SC in the pressure phase diagram. On the other hand, the CsV_3Sb_5 crystals can be exfoliated to thin flakes of a few nanometers thickness, and its CDW and superconducting state show an opposite but non-monotonic evolution with flake thickness [31, 32]: T_c is enhanced to the maximum value of 4.5 K around 30 to 60 nm and decreases to 0.9 K at 5 nm, while its non-monotonic T_{CDW} of the CDW order signals a possible 3D to 2D crossover around 60 nm. Recently, hydrostatic pressure has been successfully applied in a variety of two-dimensional materials to tune their quantum ground states, such as twisted bilayer graphene[33], transition metal dichalcogenides [34, 35], graphene/ h -BN Moiré superlattices [36], and CrI_3 [37]. In this article, we report our electrical transport measurements of mechanically exfoliated CsV_3Sb_5 thin flakes under hydrostatic pressure, to systematically compare the behaviors between the bulk and thin flakes and unveil a common mechanism of tuning the CDW and SC in CsV_3Sb_5 by pressure and dimensionality.

Several CsV_3Sb_5 thin flake devices (≈ 60 nm) on SiO_2/Si substrate have been fabricated with Ti/Au electrodes for electrical resistance measurements and encaps-

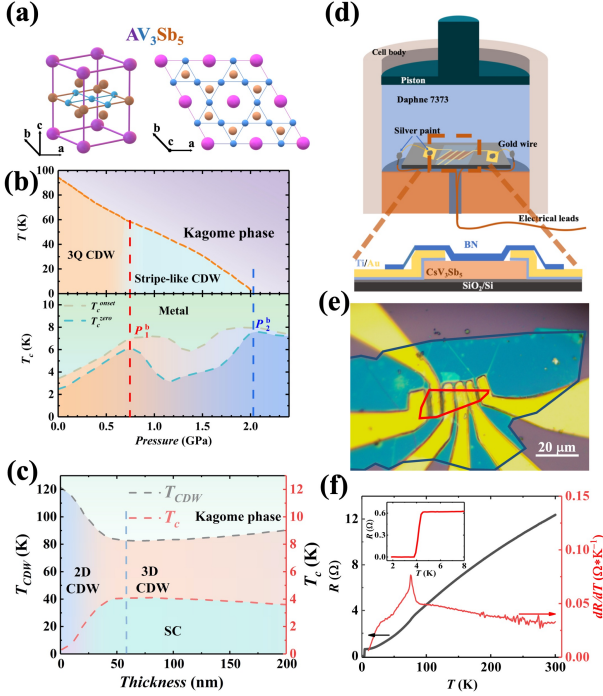


FIG. 1. Schematic illustration of crystal structure and phase diagrams of CsV₃Sb₅ and the experimental set-ups for electrical resistance measurements on CsV₃Sb₅ thin flake under pressure. **a**, Three-dimensional crystal structure of CsV₃Sb₅ on the left with its top view on the right. **b**, Phase diagrams for the bulk CsV₃Sb₅ under pressure with the CDW T_{CDW} (top), SC T_c^{onset} and T_c^{zero} (bottom) adapted from Refs. [12, 29, 30]. **c**, Thickness dependence of T_{CDW} and T_c for CsV₃Sb₅ flakes with the blue dashed line as the crossover region, adapted from Refs. [32]. **d**, Schematic illustration of the experimental set-ups, where the CsV₃Sb₅ thin flake device was encapsulated into a piston cell with Daphne 7373 as the pressure medium. The bottom of **d** shows a section view of the device structure. **e**, Optical microscopy image of the device. The CsV₃Sb₅ thin flake and *h*-BN are marked with red and blue solid lines, respectively. **f**, Temperature dependence of electrical resistance (black) $R(T)$ and its derivative (red) dR/dT of the CsV₃Sb₅ thin flake device. The inset shows the SC transition at low temperatures in the $R(T)$ curve.

insulated in a piston pressure cell. CsV₃Sb₅ thin flakes were obtained by mechanical exfoliation and all devices were prepared by the standard photolithography process. The flake thickness could be roughly estimated from its optical color in microscope and precisely confirmed by scanning AFM in tapping-mode. CsV₃Sb₅ flakes were transferred onto the Si substrate (290 nm SiO₂) by the polydimethylsiloxane (PDMS) transfer method. Ti/Au (5 nm/50 nm) films were deposited by magnetron sputtering in sequence as the electrodes for better electrical contacts. Finally, the exfoliated *h*-BN flakes were transferred onto the devices by the PDMS transfer method as a capping layer to protect the device from further

degradation during operations. The schematic figure of the experimental set-up is shown in Fig. 1(d) and the CsV₃Sb₅ thin flake and *h*-BN capping layer in the device are marked with red and blue lines, respectively, in Fig. 1(e). All the transfer processes were performed in the glove box with both oxygen and water vapor content lower than 10 ppm to avoid oxidation.

The device was diced into 1.5 mm × 1.5 mm in size to fit the inner bore of the pressure cell, as shown in Fig. 1(d). The whole device was encapsulated in a piston-cylinder-type cell with Daphne 7373 as the pressure transmitting medium and the pressure at low temperature was calibrated by the Pb superconducting transition temperature from electrical resistivity measurements. PPMS and Oxford ³He refrigerators were used to cool devices down to 1.8 K and 0.3 K, respectively, with magnetic field up to 14 T along the *c* direction. Since the device is fragile to static charge or current pulse during preservation or measurement, special cares with proper grounding should be called for.

In order to cross-check the results, high quality and well-characterized CsV₃Sb₅ single crystals were obtained from two different groups. Several CsV₃Sb₅ thin flakes from each group were prepared and they indeed show a consistent behavior under pressure. For one device, the thin CsV₃Sb₅ flake is calibrated 58.6 nm in thickness, where its T_{CDW} and T_c reaches the minimum and maximum value, respectively [32]. Fig. 1(f) shows the temperature-dependent resistance and its derivative (dR/dT) for the CsV₃Sb₅ thin flake at ambient pressure, where the kink anomaly in resistance and the corresponding peak in dR/dT signals a CDW transition at $T_{CDW} = 76$ K and a sharp superconducting transition can be observed with $T_c^{\text{onset}} = 4.4$ K and $T_c^{\text{zero}} = 3.8$ K as in the inset of Fig. 1(f). Our T_{CDW} and T_c values are consistent with the previous report for 60 nm CsV₃Sb₅ thin flakes [32].

Figure 2(a) and (c) show the temperature-dependent electrical resistance for the CsV₃Sb₅ thin flake under a series of pressures up to 2.12 GPa, illustrating the systematic evolution of SC and CDW states as a function of pressure. Similar to the bulk case, the T_{CDW} in CsV₃Sb₅ can be determined by the kink structure in the resistance curves $R(T)$ or the peak-like anomaly in the derivative resistance curves dR/dT , as in Fig. 2(e). With increased pressure, the T_{CDW} is smoothly suppressed and reaches zero at a pressure of $P_2 = 1.83$ GPa, comparable to but slightly smaller than $P_2^b \sim 2.0$ GPa in the bulk. Moreover, we notice a sudden change of the peak feature in dR/dT from a broad peak at ambient pressure to a sharp peak-dip structure at 0.09 GPa as in Fig. 2(e), and that the peak gets suppressed but the dip becomes more prominent with increased pressure until 1.83 GPa. We ascribe the change in dR/dT at 0.09 GPa in the thin flake to the same origin as those for features observed at $P_1^b \sim 0.7$ GPa in the bulk, signaling a possible transition of the

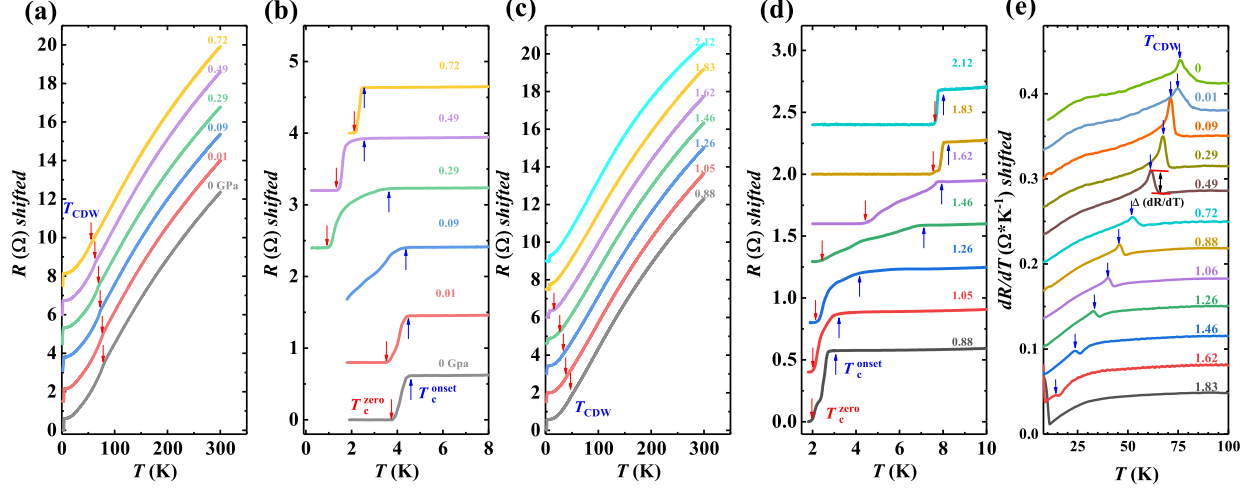


FIG. 2. Temperature dependence of the electrical resistance for the CsV_3Sb_5 thin flake device under a series of pressures. **a, c**, Temperature-dependent resistance for device No. 7 in the low and high pressure range, respectively. The CDW transition temperatures T_{CDW} are marked by red arrows. **b, d**, SC transition temperatures for the same device in the respective low and high pressure ranges, with blue and red arrows mark the T_c^{onset} and T_c^{zero} , respectively. **e**, The derivative of resistance curves, dR/dT , under various pressures. The peaks in dR/dT are marked by blue arrows, signaling the CDW T_{CDW} . All curves are vertically shifted for clarity.

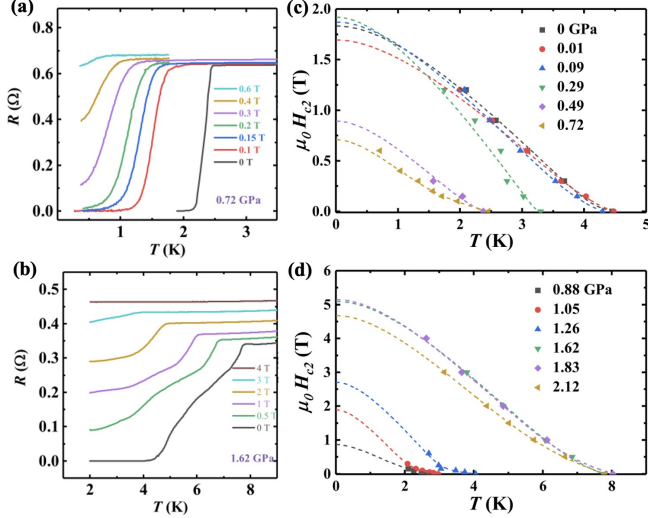


FIG. 3. Upper critical field for device No. 7 under different pressures. **a, b**, Temperature dependence of resistance under magnetic field applied along c -axis at $P = 0.72, 1.62$ GPa, respectively. **c, d**, The evolution of H_{c2} - T phase diagram (determined by T_c^{onset}) as a function of pressure. The dashed lines are two band model fitting curves[38].

CDW order. It seems that the reduced thickness of the CsV_3Sb_5 thin flake has tuned the emergent CDW order at P_1^b to be more energetically favored in a much lower pressure at $P_1 \sim 0.09$ GPa.

Figure 2(b) and (d) show the enlarged view with focus on the SC evolution in the CsV_3Sb_5 thin flake under pressure, where the red and blue arrows mark the onset and

zero-resistance transition temperatures, T_c^{onset} and T_c^{zero} , respectively. If we track the evolution of T_c^{onset} for the CsV_3Sb_5 thin flake as a function of pressure, it shows an immediate decrease upon squeezing, opposite to an initial increase of T_c^{onset} to a local maximum around 0.7 GPa in the bulk, and becomes roughly constant around 2.5 K between 0.49 and 1.05 GPa before ramping up to another local maximum of 8 K at 1.83 GPa, similar to the observation in the bulk CsV_3Sb_5 , as shown in Fig. 2(b). When comparing the superconducting behaviors between the thin flake and bulk, two local maximum T_c pressures for the double superconducting domes in the bulk CsV_3Sb_5 at $P_1^b \sim 0.7$ GPa and $P_2^b \sim 2.0$ GPa have shifted to $P_1 < 0.10$ GPa and $P_2 \sim 1.8$ GPa, respectively. In particular, the shifted P_1 value to less than 0.1 GPa also corroborates our claim that the original CDW order switch has now been tuned to 0.09 GPa in the thin flake, assuming a stronger competition between the emergent CDW and SC between P_1 and P_2 . Above P_2 , T_c^{onset} decreases together with T_c^{zero} as the CDW state vanishes.

We stress that the superconducting transitions are very broad between P_1 and P_2 , exhibiting either multiple-step or long-tail features. For example, T_c^{onset} and T_c^{zero} are 3.5 and 1.0 K, respectively, at 0.29 GPa, while they are 7.8 and 4.1 K at 1.62 GPa. The transition-width is comparable to T_c^{onset} and such a broad transition generally implies an inhomogeneous superconductivity in the flake. Since the transition becomes sharp again once the CDW order is suppressed at 1.83 GPa, extrinsic origins such as pressure inhomogeneity can be excluded. We argue that the SC inhomogeneity arises from the existence of different CDW domains with enhanced scatter-

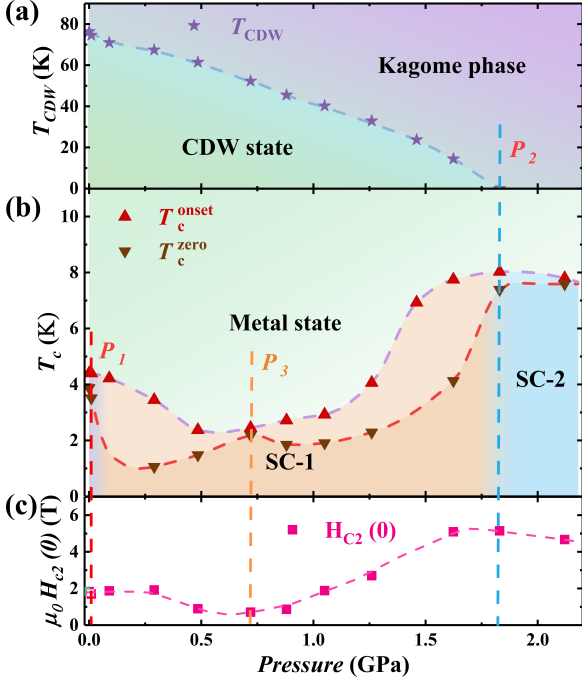


FIG. 4. **The pressure-temperature phase diagram of CsV₃Sb₅ thin flakes.** **a**, Pressure dependence of CDW transition temperatures. CDW is monotonically suppressed and vanishes at P_2 . **b**, Pressure dependence of SC transition temperatures T_c^{onset} and T_c^{zero} from $R(T)$ curves. **c**, The SC upper critical field $\mu_0 H_{c2}(0)$ as a function of pressure. $\mu_0 H_{c2}(0)$ is obtained by the two-band model fitting.

ings as in the case of bulk CsV₃Sb₅. However, the SC transition at $P_3 = 0.72$ GPa in (P_1, P_2) is sharp with $\Delta T_c = T_c^{\text{onset}} - T_c^{\text{zero}} = 0.3$ K, and such behavior is absent in the bulk CsV₃Sb₅, suggesting a homogeneous CDW order at 0.72 GPa for the thin flake.

Figure 3 illustrates the suppression of superconductivity under an applied magnetic field along the c-axis for CsV₃Sb₅ thin flakes, where the superconducting transition gets widened under magnetic field, indicative of increased inhomogeneity of SC. To study the zero-temperature upper critical field ($\mu_0 H_{c2}(0)$), and its evolution with pressure, the onset of superconductivity in the field was defined as its T_c and its dependence with temperature was fit using a two-band model[38]. An enhancement in both $\mu_0 H_{c2}(0)$ and T_c around 1.8 GPa corresponds to the state in the absence of CDW order. Additionally, a sharp superconducting transition and a local minimum of $\mu_0 H_{c2}(0)$ at 0.72 GPa suggest a competitive yet coexisting relationship between the superconducting state and CDW order.

The pressure-dependent phase diagrams of CDW (T_{CDW}) and SC (T_c^{onset} and T_c^{zero}) in CsV₃Sb₅ thin flakes are plotted in Fig.4(a) and (b), based on the electri-

cal resistance measurements under pressure, in comparison with its bulk form as in Fig.1(b). Even though the CDW order still decreases monotonically with pressure and completely disappears at $P_2 \sim 1.8$ GPa with a similar T_c maximum as in the bulk, the SC in CsV₃Sb₅ thin flakes show a remarkably different behavior. The bulk CsV₃Sb₅ displays an M-shaped double superconducting domes and a shallow T_c valley in between, with its two local T_c maximum at $P_1^b \sim 0.7$ GPa and $P_2^b \sim 2.0$ GPa, respectively. For CsV₃Sb₅ thin flakes, however, the higher-pressure SC dome is barely changed while the lower-pressure SC dome centered around 0.7 GPa in the bulk has been lowered to the ambient pressure, $P_1 < 0.1$ GPa. As in Fig.4(b), T_c^{zero} decreases rapidly above ambient pressure while T_c^{onset} changes little in a small pressure range of 0.1 GPa, which resembles well with the bulk around $P_1^b \sim 0.7$ GPa. We argue that the original CDW switch at 0.7 GPa has shifted to below 0.1 GPa due to the reduced thickness in the thin flake, and causes a change of the SC phase diagram in accordance [10, 29]. Moreover, the superconducting T_c^{onset} and T_c^{zero} are connected at P_1 and P_2 , and form a loop, which is divided into two separate lobes by a node at $P_3 \sim 0.72$ GPa. In each lobe, the presence of CDW domains yield an inhomogeneous SC with a broad transition due to the strong competition between SC and CDW as in the case of 1T-TaSe₂ [39]. When magnetic field is applied perpendicular to the CsV₃Sb₅ thin flake, its upper critical field $\mu_0 H_{c2}(0)$ as a function of pressure is plotted in Fig.4(c), showing a weakened double-dome structure compared with the bulk (The temperature-dependent resistance curves are included in Fig. 3 (c, d) for different fields and the $\mu_0 H_{c2}(0)$ at zero Kelvin can be obtained by a two-band model fitting[38]).

Our experimental results can be explained by the tuning of CDW orders with reduced dimensionality in the CsV₃Sb₅ thin flake. The CDW in CsV₃Sb₅ at ambient pressure has been reported to evolve from 3D to 2D in nature with reduced sample thickness as in Fig.1(c), where the vanishing of the A_{1g} Raman frequency shift is observed below a critical thickness of 25 layers, signaling a weakened electron-phonon coupling[32]. For the CsV₃Sb₅ thin flake, reduced thickness would reduce the interlayer coupling and suppress the 3D CDW ordering along the c axis, but friendly to the 2D CDW instead. On the other hand, for the bulk, recent NMR results claim that the 3Q-CDW state should be dominant at the pressure below P_1^b , with a 3D character due to interlayer couplings, and transforms into a 2D stripe-like CDW with a unidirectional $4a_0$ modulation under a moderate pressure in (P_1^b, P_2^b) , as in Fig.1(b) [30]. The 3Q- and stripe-like CDWs should be very close in energy and compete for the electronic ground state in CsV₃Sb₅[30], and the vertical Cs-Sb atomic distance is more sensitive to the hydrostatic pressure, resulting in a dominant reduction of the c/a ratio[12]. In such a case, the 3Q CDW may lift its

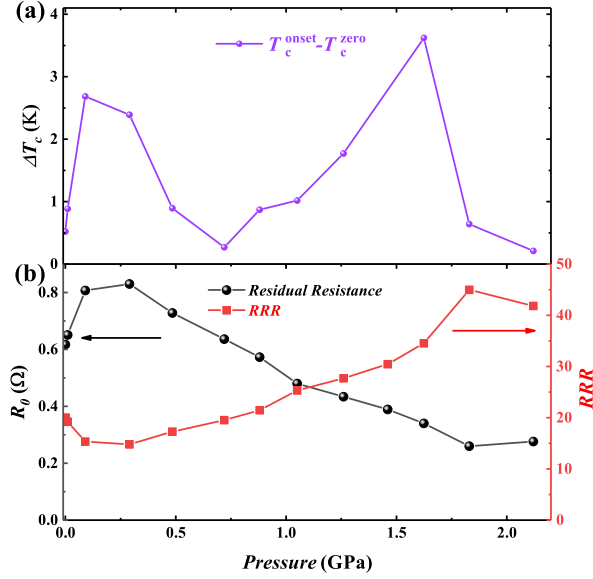


FIG. 5. **Pressure dependence of $\Delta(T_c)$, residual resistance and residual-resistance ratio for the CsV₃Sb₅ thin flake.** **a**, $\Delta(T_c)$ as a function of pressure (determined by $T_c^{\text{onset}} - T_c^{\text{zero}}$ for device No. 7). **b**, Pressure dependence of residual resistance and residual-resistance ratio (RRR), where the residual resistance is defined by the resistance value at 10 K for the specific pressure.

energy due to interlayer couplings and yield to the stripe-like CDW around P_1^b [40, 41]. We speculate that the 2D CDW in CsV₃Sb₅ thin flake and stripe-like CDW for the bulk should be identical in origin and antagonistic to the SC, causing the SC valley in pressure phase diagrams. In such a scenario, the dimensionality and hydrostatic pressure may play the same role in tuning the ground state of CsV₃Sb₅. Even though our first-principle calculation on the phonon modes for the bulk CsV₃Sb₅ under pressure and a bilayer slab can not explicitly identify the CDW transition, it suggests the delicate competition between different CDW orders with different stacking modulation and a robust feature of the in-plane distortion (see section 4 in Supplemental Material) [42]. Because our CsV₃Sb₅ thin flake is close to crossover thickness from 3D to 2D CDW, it is natural to expect the CDW switch would be lowered to only < 0.1 GPa under pressure and the corresponding SC T_c peak should be observed at the new P_1 .

We note that STM measurements have reported a stripe-like charge order with $4a_0/3$ spatial modulation on the surface of bulk CsV₃Sb₅ and its relation with the stripe-like CDW between (P_1^b, P_2^b) is not clear yet [16, 17]. Moreover, the T_c of CsV₃Sb₅ thin flakes below 1.8 GPa is relatively lower than the bulk, indicating a more intense competition between SC and 2D CDW with reduced sample thickness. The coexistence of stripe-like CDW and SC has also been observed in the high-

T_c cuprate superconductors La_{2-x}Ba_xCuO₄, and pair-density-wave (PDW) SC has been proposed with non-zero momentum for Cooper pairs [1, 2]. For other layered superconductors such as Ising superconductor NbSe₂, its T_c decreases from 7.2 K in the bulk to 3 K for monolayer with reduced sample thickness, while its T_{CDW} shows an opposite increase from 33 K to 145 K [6, 43–45]. However, when CDW is suppressed in NbSe₂ by increasing the interlayer distance, the T_c seems robust against the change of sample thickness [46]. We observe that the T_c for CsV₃Sb₅ thin flakes at P_2 (where CDW vanishes) is also comparable to the bulk value. We thus argue the variation of T_c with thickness is probably due to the thickness-modulated CDW competing with superconductivity. It is intriguing to explore possible PDW SC at ambient pressure and the pressure phase diagram for thinner CsV₃Sb₅ flakes to check whether the SC T_c can be recovered back to the bulk value when CDW is totally suppressed [32].

In summary, we have systematically investigate electrical resistance of the CsV₃Sb₅ thin flakes (58nm) under pressure to compare its pressure phase diagram with the bulk. In contrast to the M-shaped double SC domes, the CDW switch and first SC T_c dome have shifted to below 0.1 GPa in the thin flake from the initial $P_1^b \sim 0.7$ GPa as in the bulk. We would thus conclude that the hydrostatic pressure or sample thickness can both tune the subtle competition and balance between the 3D and 2D CDWs in CsV₃Sb₅ due to the interlayer interactions and the SC response to the CDW switch accordingly. Considering the complex relationship between CDW and SC competition in CsV₃Sb₅ thin flakes, we believe it is necessary to conduct low-temperature Raman spectroscopy under pressure for further studies, as in the case of 2H-TaS₂ [47]. Furthermore, in order to shed more light on the nature of 3D and 2D CDW, it is worth to explore the evolution of CDW and SC for monolayer or multilayer CsV₃Sb₅ under pressure in the future.

This work was supported by the National Key R&D Program of China (Grant No. 2022YFA1402200), the National Natural Science Foundation of China (Grant No. 12174333 and 12274364), and the Key R&D Program of Zhejiang Province, China (Grant No. 2021C01002). X.X. acknowledges the financial support from National Natural Science Foundation of China (Grants No. 12274369 and No. 11974061).

* ccao@zju.edu.cn

† xinluphy@zju.edu.cn

- [1] M. Hücker, M. v. Zimmermann, G. D. Gu, Z. J. Xu, J. S. Wen, G. Xu, H. J. Kang, A. Zheludev, and J. M. Tranquada, Stripe order in superconducting La_{2-x}Ba_xCuO₄ ($0.095 \leq x \leq 0.155$), *Phys. Rev. B* **83**, 104506 (2011).
- [2] Q. Li, M. Hücker, G. D. Gu, A. M. Tsvelik,

- and J. M. Tranquada, Two-dimensional superconducting fluctuations in stripe-ordered $\text{La}_{1.875}\text{Ba}_{0.125}\text{CuO}_4$, *Phys. Rev. Lett.* **99**, 067001 (2007).
- [3] J. Fink, E. Schierle, E. Weschke, J. Geck, D. Hawthorn, V. Soltwisch, H. Wadati, H.-H. Wu, H. A. Dürr, N. Wizen, B. Büchner, and G. A. Sawatzky, Charge ordering in $\text{La}_{1.8-x}\text{Eu}_{0.2}\text{Sr}_x\text{CuO}_4$ studied by resonant soft x-ray diffraction, *Phys. Rev. B* **79**, 100502 (2009).
- [4] Y. Ihara, K. Moribe, S. Fukuoka, and A. Kawamoto, Microscopic coexistence of superconductivity and charge order in the organic superconductor $\beta'' - (\text{BEDT} - \text{TTF})_4[(\text{H}_3\text{O})\text{Ga}(\text{C}_2\text{O}_4)_3]\text{C}_6\text{H}_5\text{NO}_2$, *Phys. Rev. B* **100**, 060505 (2019).
- [5] N. Morinaka, K. Takahashi, R. Chiba, F. Yoshikane, S. Niizeki, M. Tanaka, K. Yakushi, M. Koeda, M. Hedo, T. Fujiwara, Y. Uwatoko, Y. Nishio, K. Kajita, and H. Mori, Superconductivity competition with checkerboard-type charge ordering in the organic conductor $\beta - (\text{meso} - \text{DMBEDT} - \text{TTF})_2\text{PF}_6$, *Phys. Rev. B* **80**, 092508 (2009).
- [6] X. Xi, L. Zhao, Z. Wang, H. Berger, L. Forró, J. Shan, and K. F. Mak, Strongly enhanced charge-density-wave order in monolayer NbSe_2 , *Nature Nanotechnology* **10**, 765 (2015).
- [7] J. A. Galvis, P. Rodière, I. Guillamon, M. R. Osorio, J. G. Rodrigo, L. Cario, E. Navarro-Moratalla, E. Coronado, S. Vieira, and H. Suderow, Scanning tunneling measurements of layers of superconducting $2h\text{-tase}_2$: Evidence for a zero-bias anomaly in single layers, *Phys. Rev. B* **87**, 094502 (2013).
- [8] B. R. Ortiz, L. C. Gomes, J. R. Morey, M. Winiarski, M. Bordelon, J. S. Mangum, I. W. H. Oswald, J. A. Rodriguez-Rivera, J. R. Neilson, S. D. Wilson, E. Ertekin, T. M. McQueen, and E. S. Toberer, New kagome prototype materials: discovery of KV_3Sb_5 , RbV_3Sb_5 , and CsV_3Sb_5 , *Phys. Rev. Materials* **3**, 094407 (2019).
- [9] B. R. Ortiz, P. M. Sarte, E. M. Kenney, M. J. Graf, S. M. L. Teicher, R. Seshadri, and S. D. Wilson, Superconductivity in the \mathbb{Z}_2 kagome metal KV_3Sb_5 , *Phys. Rev. Materials* **5**, 034801 (2021).
- [10] B. R. Ortiz, S. M. L. Teicher, Y. Hu, J. L. Zuo, P. M. Sarte, E. C. Schueller, A. M. M. Abeykoon, M. J. Krogstad, S. Rosenkranz, R. Osborn, R. Seshadri, L. Balents, J. He, and S. D. Wilson, CsV_3Sb_5 : A \mathbb{Z}_2 topological kagome metal with a superconducting ground state, *Phys. Rev. Lett.* **125**, 247002 (2020).
- [11] Q. Yin, Z. Tu, C. Gong, Y. Fu, S. Yan, and H. Lei, Superconductivity and normal-state properties of kagome metal RbV_3Sb_5 single crystals, *Chinese Physics Letters* **38**, 037403 (2021).
- [12] K. Y. Chen, N. N. Wang, Q. W. Yin, Y. H. Gu, K. Jiang, Z. J. Tu, C. S. Gong, Y. Uwatoko, J. P. Sun, H. C. Lei, J. P. Hu, and J.-G. Cheng, Double superconducting dome and triple enhancement of T_c in the kagome superconductor CsV_3Sb_5 under high pressure, *Phys. Rev. Lett.* **126**, 247001 (2021).
- [13] H. Li, T. T. Zhang, T. Yilmaz, Y. Y. Pai, C. E. Marvinney, A. Said, Q. W. Yin, C. S. Gong, Z. J. Tu, E. Vescovo, C. S. Nelson, R. G. Moore, S. Murakami, H. C. Lei, H. N. Lee, B. J. Lawrie, and H. Miao, Observation of unconventional charge density wave without acoustic phonon anomaly in kagome superconductors AV_3Sb_5 ($A = \text{Rb}, \text{Cs}$), *Phys. Rev. X* **11**, 031050 (2021).
- [14] F. Du, S. Luo, B. R. Ortiz, Y. Chen, W. Duan, D. Zhang, X. Lu, S. D. Wilson, Y. Song, and H. Yuan, Pressure-induced double superconducting domes and charge instability in the kagome metal KV_3Sb_5 , *Phys. Rev. B* **103**, L220504 (2021).
- [15] Y.-X. Jiang, J.-X. Yin, M. M. Denner, N. Shumiya, B. R. Ortiz, G. Xu, Z. Guguchia, J. He, M. S. Hossain, X. Liu, J. Ruff, L. Kautzsch, S. S. Zhang, G. Chang, I. Belopolski, Q. Zhang, T. A. Cochran, D. Multer, M. Litskevich, Z.-J. Cheng, X. P. Yang, Z. Wang, R. Thomale, T. Neupert, S. D. Wilson, and M. Z. Hasan, Unconventional chiral charge order in kagome superconductor KV_3Sb_5 , *Nature Materials* **20**, 1353 (2021).
- [16] H. Zhao, H. Li, B. R. Ortiz, S. M. L. Teicher, T. Park, M. Ye, Z. Wang, L. Balents, S. D. Wilson, and I. Zeljkovic, Cascade of correlated electron states in the kagome superconductor CsV_3Sb_5 , *Nature* **599**, 216 (2021).
- [17] H. Chen, H. Yang, B. Hu, Z. Zhao, J. Yuan, Y. Xing, G. Qian, Z. Huang, G. Li, Y. Ye, S. Ma, S. Ni, H. Zhang, Q. Yin, C. Gong, Z. Tu, H. Lei, H. Tan, S. Zhou, C. Shen, X. Dong, B. Yan, Z. Wang, and H.-J. Gao, Roton pair density wave in a strong-coupling kagome superconductor, *Nature* **599**, 222 (2021).
- [18] Z. Liang, X. Hou, F. Zhang, W. Ma, P. Wu, Z. Zhang, F. Yu, J.-J. Ying, K. Jiang, L. Shan, Z. Wang, and X.-H. Chen, Three-dimensional charge density wave and surface-dependent vortex-core states in a kagome superconductor CsV_3Sb_5 , *Phys. Rev. X* **11**, 031026 (2021).
- [19] Z. Wang, S. Ma, Y. Zhang, H. Yang, Z. Zhao, Y. Ou, Y. Zhu, S. Ni, Z. Lu, H. Chen, K. Jiang, L. Yu, Y. Zhang, X. Dong, J. Hu, H.-J. Gao, and Z. Zhao, Distinctive momentum dependent charge-density-wave gap observed in CsV_3Sb_5 superconductor with topological kagome lattice, *arxiv* **2104**, 05556 (2021).
- [20] K. Nakayama, Y. Li, T. Kato, M. Liu, Z. Wang, T. Takahashi, Y. Yao, and T. Sato, Multiple energy scales and anisotropic energy gap in the charge-density-wave phase of the kagome superconductor CsV_3Sb_5 , *Phys. Rev. B* **104**, L161112 (2021).
- [21] Z. Liu, N. Zhao, Q. Yin, C. Gong, Z. Tu, M. Li, W. Song, Z. Liu, D. Shen, Y. Huang, K. Liu, H. Lei, and S. Wang, Charge-density-wave-induced bands renormalization and energy gaps in a kagome superconductor RbV_3Sb_5 , *Phys. Rev. X* **11**, 041010 (2021).
- [22] Y. Hu, X. Wu, B. R. Ortiz, X. Han, N. C. Plumb, S. D. Wilson, A. P. Schnyder, and M. Shi, Coexistence of trihexagonal and star-of-david pattern in the charge density wave of the kagome superconductor AV_3Sb_5 , *Phys. Rev. B* **106**, L241106 (2022).
- [23] B. R. Ortiz, S. M. L. Teicher, L. Kautzsch, P. M. Sarte, N. Ratcliff, J. Harter, J. P. C. Ruff, R. Seshadri, and S. D. Wilson, Fermi surface mapping and the nature of charge-density-wave order in the kagome superconductor CsV_3Sb_5 , *Phys. Rev. X* **11**, 041030 (2021).
- [24] Q. Stahl, D. Chen, T. Ritschel, C. Shekhar, E. Sadrollahi, M. C. Rahn, O. Ivashko, M. v. Zimmermann, C. Felser, and J. Geck, Temperature-driven reorganization of electronic order in CsV_3Sb_5 , *Phys. Rev. B* **105**, 195136 (2022).
- [25] J. Luo, Z. Zhao, Y. Z. Zhou, J. Yang, A. F. Fang, H. T. Yang, H. J. Gao, R. Zhou, and G.-q. Zheng, Possible star-of-david pattern charge density wave with

- additional modulation in the kagome superconductor CsV_3Sb_5 , *npj Quantum Materials* **7**, 30 (2022).
- [26] C. Mielke, D. Das, J. X. Yin, H. Liu, R. Gupta, Y. X. Jiang, M. Medarde, X. Wu, H. C. Lei, J. Chang, P. Dai, Q. Si, H. Miao, R. Thomale, T. Neupert, Y. Shi, R. Khasanov, M. Z. Hasan, H. Luetkens, and Z. Guguchia, Time-reversal symmetry-breaking charge order in a kagome superconductor, *Nature* **602**, 245 (2022).
- [27] R. Khasanov, D. Das, R. Gupta, C. Mielke, M. Elender, Q. Yin, Z. Tu, C. Gong, H. Lei, E. T. Ritz, R. M. Fernandes, T. Birol, Z. Guguchia, and H. Luetkens, Time-reversal symmetry broken by charge order in CsV_3Sb_5 , *Phys. Rev. Res.* **4**, 023244 (2022).
- [28] N. Ratcliff, L. Hallett, B. R. Ortiz, S. D. Wilson, and J. W. Harter, Coherent phonon spectroscopy and interlayer modulation of charge density wave order in the kagome metal CsV_3Sb_5 , *Phys. Rev. Mater.* **5**, L111801 (2021).
- [29] F. H. Yu, D. H. Ma, W. Z. Zhuo, S. Q. Liu, X. K. Wen, B. Lei, J. J. Ying, and X. H. Chen, Unusual competition of superconductivity and charge-density-wave state in a compressed topological kagome metal, *Nature Communications* **12**, 3645 (2021).
- [30] L. Zheng, Z. Wu, Y. Yang, L. Nie, M. Shan, K. Sun, D. Song, F. Yu, J. Li, D. Zhao, S. Li, B. Kang, Y. Zhou, K. Liu, Z. Xiang, J. Ying, Z. Wang, T. Wu, and X. Chen, Emergent charge order in pressurized kagome superconductor CsV_3Sb_5 , *Nature* **611**, 682 (2022).
- [31] Y. Song, T. Ying, X. Chen, X. Han, X. Wu, A. P. Schnyder, Y. Huang, J.-g. Guo, and X. Chen, Competition of superconductivity and charge density wave in selective oxidized CsV_3Sb_5 thin flakes, *Phys. Rev. Lett.* **127**, 237001 (2021).
- [32] B. Song, T. Ying, X. Wu, W. Xia, Q. Yin, Q. Zhang, Y. Song, X. Yang, J. Guo, L. Gu, X. Chen, J. Hu, A. P. Schnyder, H. Lei, Y. Guo, and S. Li, Anomalous enhancement of charge density wave in kagome superconductor CsV_3Sb_5 approaching the 2D limit, *Nature Communications* **14**, 2492 (2023).
- [33] M. Yankowitz, S. Chen, H. Polshyn, Y. Zhang, K. Watanabe, T. Taniguchi, D. Graf, A. F. Young, and C. R. Dean, Tuning superconductivity in twisted bilayer graphene, *Science* **363**, 1059 (2019).
- [34] Z. Zhao, H. Zhang, H. Yuan, S. Wang, Y. Lin, Q. Zeng, G. Xu, Z. Liu, G. K. Solanki, K. D. Patel, Y. Cui, H. Y. Hwang, and W. L. Mao, Pressure induced metallization with absence of structural transition in layered molybdenum diselenide, *Nature Communications* **6**, 7312 (2015).
- [35] P. Ci, Y. Chen, J. Kang, R. Suzuki, H. S. Choe, J. Suh, C. Ko, T. Park, K. Shen, Y. Iwasa, S. Tongay, J. W. I. Ager, L.-W. Wang, and J. Wu, Quantifying van der Waals interactions in layered transition metal dichalcogenides from pressure-enhanced valence band splitting, *Nano Letters* **17**, 4982 (2017).
- [36] M. Yankowitz, J. Jung, E. Laksono, N. Leconte, B. L. Chittari, K. Watanabe, T. Taniguchi, S. Adam, D. Graf, and C. R. Dean, Dynamic band-structure tuning of graphene moiré superlattices with pressure, *Nature* **557**, 404 (2018).
- [37] T. Song, Z. Fei, M. Yankowitz, Z. Lin, Q. Jiang, K. Hwangbo, Q. Zhang, B. Sun, T. Taniguchi, K. Watanabe, M. A. McGuire, D. Graf, T. Cao, J.-H. Chu, D. H. Cobden, C. R. Dean, D. Xiao, and X. Xu, Switching 2d magnetic states via pressure tuning of layer stacking, *Nature Materials* **18**, 1298 (2019).
- [38] A. Gurevich, Enhancement of the upper critical field by nonmagnetic impurities in dirty two-gap superconductors, *Phys. Rev. B* **67**, 184515 (2003).
- [39] Y. I. Joe, X. M. Chen, P. Ghaemi, K. D. Finkelstein, G. A. de la Peña, Y. Gan, J. C. T. Lee, S. Yuan, J. Geck, G. J. MacDougall, T. C. Chiang, S. L. Cooper, E. Fradkin, and P. Abbamonte, Emergence of charge density wave domain walls above the superconducting dome in $1T\text{-TiSe}_2$, *Nature Physics* **10**, 421 (2014).
- [40] A. A. Tsirlin, P. Fertey, B. R. Ortiz, B. Klis, V. Merkl, M. Dressel, S. D. Wilson, and E. Uykur, Role of sb in the superconducting kagome metal CsV_3Sb_5 revealed by its anisotropic compression, *SciPost Phys.* **12**, 049 (2022).
- [41] T. Neupert, M. M. Denner, J.-X. Yin, R. Thomale, and M. Z. Hasan, Charge order and superconductivity in kagome materials, *Nature Physics* **18**, 137 (2022).
- [42] C. Park and Y.-W. Son, Condensation of preformed charge density waves in kagome metals, *arxiv* **2303**, 08598 (2023).
- [43] Q. H. Wang, K. Kalantar-Zadeh, A. Kis, J. N. Coleman, and M. S. Strano, Electronics and optoelectronics of two-dimensional transition metal dichalcogenides, *Nature Nanotechnology* **7**, 699 (2012).
- [44] M. Chhowalla, H. S. Shin, G. Eda, L.-J. Li, K. P. Loh, and H. Zhang, The chemistry of two-dimensional layered transition metal dichalcogenide nanosheets, *Nature Chemistry* **5**, 263 (2013).
- [45] X. Xi, Z. Wang, W. Zhao, J.-H. Park, K. T. Law, H. Berger, L. Forró, J. Shan, and K. F. Mak, Ising pairing in superconducting NbSe_2 atomic layers, *Nature Physics* **12**, 139 (2016).
- [46] H. Zhang, A. Rousuli, K. Zhang, L. Luo, C. Guo, X. Cong, Z. Lin, C. Bao, H. Zhang, S. Xu, R. Feng, S. Shen, K. Zhao, W. Yao, Y. Wu, S. Ji, X. Chen, P. Tan, Q.-K. Xue, Y. Xu, W. Duan, P. Yu, and S. Zhou, Tailored ising superconductivity in intercalated bulk NbSe_2 , *Nature Physics* **10.1038/s41567-022-01778-7** (2022).
- [47] R. Grasset, Y. Gallais, A. Sacuto, M. Cazayous, S. Mañas Valero, E. Coronado, and M.-A. Méasson, Pressure-induced collapse of the charge density wave and higgs mode visibility in 2H-TaS_2 , *Phys. Rev. Lett.* **122**, 127001 (2019).